JOURNAL OF MATERIALS SCIENCE 31 (1996) 5351–5361

The effect of Al_2O_3 particulates on the precipitation behaviour of 6061 aluminium-matrix composites

T. DAS*, P. R. MUNROE, S. BANDYOPADHYAY
School of Materials Science and Engineering, University of New South Wales, Sydney, New South Wales 2052, Australia

The effect of angular and spherical shaped Al_2O_3 particulates on the precipitation behaviour of 6061 aluminium-matrix composites has been studied using microhardness testing, differential scanning calorimetry (DSC) and transmission electron microscopy (TEM). The evolution of precipitates at each stage of precipitation corresponding to the DSC-peak was monitored through careful TEM observations. Both the formation and dissolution behaviour of the precipitates in the ageing process in the composites were compared with the unreinforced 6061 matrix alloy. Although an overall accelerated ageing response in the composites was reported, not all stages in the ageing process were influenced by the addition of particulates. However, the precipitation sequence was not altered by the presence of the particulates. The degree of acceleration and the relative proportion of the phase/phases was found to depend on reinforcement parameters such as size, shape and volume fraction. In the composites, higher dislocation densities were observed in the immediate vicinity of the ceramic particles which may have formed due to the large difference in the coefficients of thermal expansion (CTE) between the ceramic particles and the matrix. These CTE–dislocation effects influence the kinetics of precipitation.

1. Introduction

Aluminium-based metal-matrix composites offer the prospect of materials with high specific stiffness, which make them potentially attractive to the aerospace and automotive industries. Many of these composites are based upon age-hardenable aluminium alloys reinforced with ceramic particulates such as SiC and Al_2O_3. It is well known that these particles may accelerate the ageing kinetics of the matrix alloy [1–11]. This acceleration is associated with the higher matrix dislocation densities observed in these composites through differential thermal expansion between the matrices and their ceramic reinforcements. Matrix dislocations may act as nucleation sites for precipitates, and the higher densities commonly observed in such composites facilitate enhanced precipitate formation. In addition, the dislocations may act as preferential paths for solute diffusion further accelerating the ageing process. Elastic strains in the matrix, associated with the presence of the reinforcements may also lead to stress-assisted solute diffusion.

There have been several studies of the ageing behaviour of particulate-reinforced aluminium metal-matrix composites based on a 6xxx series matrix [1–9]. Most of these studies have examined the effect of SiC reinforcements on the kinetics of precipitation. However, Dutta *et al.* [4] investigated the effect of 10 and 15 vol % alumina particulates on the ageing behaviour of 6061, and Hadianfard *et al.* [7], Unsworth and Bandyopadhyay [8] and Edwards *et al.* [9] studied the precipitation kinetics of a composite called Comral-85, based on a 6061 matrix reinforced with 20 vol % alumina-based microsphere particulates. In general, it has been shown that the addition of either SiC or Al_2O_3 particulates accelerates the ageing process, but without altering the precipitation sequence. Furthermore, the presence of the particulates also increases the peak hardness achieved. Although these reinforcements do not appear to alter the precipitation sequence, Dutta *et al.* [4] showed that the relative volume fractions of precipitates which formed were affected by the presence of the reinforcement. However, the effects of particulate parameters, such as the volume fraction of reinforcement, particle size and shape, on the precipitation process have so far received little attention.

In this study, the precipitation behaviour of a number of composites based on an Al-6061 matrix containing a range of volume fractions from 10–20 vol % Al_2O_3 irregular particulates was studied. In addition, a composite based upon an Al-6061 matrix containing a 20% volume fraction of spherical particles (Comral-85) was studied. This therefore allows the effects of particulate volume fraction and also the effect of particle shape on the precipitation behaviour of 6061 to be studied. The behaviour of all these composites was

* *Present address*: BHP Research, Melbourne Laboratories, Wellington Road, Mulgrave, Victoria 3170, Australia.

0022–2461

compared with the unreinforced matrix alloy. The ageing behaviour of these alloys was studied by microhardness, differential scanning calorimetry (DSC) and transmission electron microscopy (TEM).

2. Experimental procedure

2.1. Materials

The materials used in this paper were composites based on an Al-6061 matrix. These contained a 10%, 15% or 20% volume fraction of Al_2O_3 particulates, which were non-uniform in shape and had an average diameter of 12 μm. A fourth composite, termed Comral-85, was based upon an Al-6061 matrix, but contained 20% volume fraction of fine-grained polycrystalline Al_2O_3-based ceramic microspheres with an average diameter of 17.4 μm. In addition, the unreinforced matrix alloy was studied. All materials were provided in the form of 19 mm diameter extruded rods by Comalco Research Centre (CRC), Melbourne, Australia. The unreinforced 6061 aluminium alloy was direct-chill-cast at CRC and then hot extruded. The composites containing the alumina particulate, obtained from Dural Aluminium Corporation, San Diego, CA, USA, were processed by a proprietary casting route [12]. Following casting and homogenizing, the composites were hot extruded at 450 °C to 19 mm diameter rods. Comral-85 was also produced by CRC, Melbourne through a casting route. The billets were then cut into two halves and hot extruded at 460 °C using a 3000 tonne extrusion press with an extrusion ratio 38:1 and a speed 7–20 m min^{-1} to form the final 19 mm diameter rods [13]. The compositions of the matrices of composites and the monolithic alloy were determined using CAMECA SX50 electron probe micro-analyser (EPMA) on highly polished surfaces of the specimens. The average composition obtained from six different readings for all materials are listed in Table I.

2.2. Methods

The as-received materials were solution heat treated prior to microhardness testing, DSC or TEM analysis. All the samples were heat treated at 530 ± 1 °C for 2 h and quenched into iced water. They were then stored at − 15 °C before further experiments were performed.

To investigate the age-hardening behaviour of these alloys, samples from all five materials were heat treated at 175 ± 1 °C for a range of times up to 90 h. Vickers' microhardness testing was performed using a 100 g indentor load; details have been published elsewhere [14].

DSC experiments were performed on a DuPont 910 DSC unit with a DuPont 2100 thermal analyser. The samples used were discs ~0.5 mm thick and 5.00 mm diameter which were electro-discharge machined (EDM) from the bulk material. The discs were solution heat treated, as described above, prior to testing. Annealed high-purity aluminium discs were used in the reference pan for the DSC runs. All tests were started at 40 °C and terminated at 540 °C, and a constant heating rate of 20 °C min^{-1} was used. The heat flow versus temperature data were continuously stored in a computer interfaced with the calorimeter. In order to ascertain the reproducibility, at least three DSC runs were typically made for each type of sample. The 2 °C variation in peak temperatures falls within predetermined experimental tolerance of peak-temperature measurements.

TEM studies were performed to correlate microstructural changes in these materials with the peaks obtained in the DSC thermograms. Specimens for TEM investigation were obtained from a simulated thermal treatment which consisted of heating the specimens to the peak temperatures of interest, maintaining the same heating rate of 20 °C min^{-1} as employed in the DSC experimentation. Upon reaching the peak temperature, the specimens were quenched in iced water at 0 °C to preserve the microstructure. Specimens of monolithic 6061 aluminium alloy and two composites, one containing angular reinforcements (15% V_f Al_2O_3) and Comral-85 were studied. Thin slices, 0.5 mm thick, were cut along the cross-section of the extruded rods using a low-speed diamond saw. Specimens of 3 mm diameter discs were spark-cut from those thin slices by EDM. The discs were then ground to 30–40 μm thickness on 600 grit SiC-paper. Thin foils were then jet polished to perforation using a Struers Tenupol electropolishing unit. A polishing solution of 20% HNO_3 in methanol at a temperature of − 30 °C was used. Polishing was carried out under a voltage of 25 V for the composites and 11 V for the monolithic alloy. Microstructural studies and phase identification were carried out using a Jeol 2000FX transmission electron microscope (TEM) operated at 200 kV furnished with an energy dispersive X-ray spectrometer (EDS).

3. Results and discussion

Results from microhardness measurements as a function of ageing time at 175 °C for the monolithic alloy

TABLE I Chemical compositions of the monolithic 6061 aluminium alloy and the matrices of composites as determined by EPMA

Materials	Chemical composition (wt%)							
	Mg	Si	Fe	Cr	Cu	Mn	Ti	Al (bal.)
6061	0.690	0.549	0.022	0.065	0.168	0.094	0.017	98.835
10% Al_2O_3	0.819	0.507	0.037	0.083	0.173	0.009	0.007	98.472
15% Al_2O_3	0.752	0.490	0.040	0.098	0.320	0.012	0.004	98.332
20% Al_2O_3	0.756	0.508	0.066	0.119	0.282	0.004	0.001	98.197
Comral 85	0.704	0.569	0.057	0.090	0.322	0.007	0.010	98.107

and two composites, one containing 15% V_f Al_2O_3 angular reinforcements and the other containing 20% V_f Al_2O_3 spherical reinforcements (Comral-85), are shown in Fig. 1. Previous study [14] on these composites showed that the presence of particles makes a contribution to the hardness of the composite matrix, the degree of which depends on the size and distribution of the particles and also the indentation load. An indentation load of 100 g was found suitable, and matrix regions free from clusters of particles were selected for indentation to minimize the scatter in the microhardness results. Some scatter in the hardness results could not be avoided because of the presence of particles below the surface of indentation.

From the three curves in Fig. 1, differences in the behaviour of the composites and the monolithic alloy were observed. The solution-treated and as-quenched microhardness of both composites were higher than the monolithic alloy, and hardness also increased with increasing reinforcement volume fraction. The time to reach the maximum hardness was less in both composites (8 h) as compared to the monolithic alloy (10 h). Moreover, the differences between the hardness of the composites and the monolithic alloy were larger prior to the hardness maxima; beyond this peak, as the materials overaged, the differences in hardness became smaller. These observations are broadly consistent with the work of Badini *et al.* [3] and Dutta *et al.* [4] on similar materials. Some differences between this current work and previous studies in the peak ageing times and maximum hardness achieved are probably attributable to the different solution-treatment and ageing temperatures, matrix composition and the size and type of the reinforcements used.

Prior to ageing, the alloys were solution heat treated and quenched into iced water. During quenching, the differential coefficient of thermal expansion (CTE) between the matrix and the reinforcements resulted in the formation of regions of high dislocation density in the matrix, especially in regions adjacent to the reinforcement particles. Fig. 2a shows the matrix regions adjacent to a spherical particulate in Comral-85. A region of high dislocation density (2×10^{14} m^{-2}) was observed in the matrix region adjacent to the particle. However, the density of dislocations was observed to decrease with increasing distance from the particle–matrix interface. Similar behaviour was also observed in the 15 vol % Al_2O_3 composite. The average dislocation density (1.4×10^{14} m^{-2}) throughout the Comral-85 matrix was found to be significantly higher compared to the monolithic alloy (1×10^{14} m^{-2}) (Fig. 2b), but slightly lower than the 15% Al_2O_3 composite (1.6×10^{14} m^{-2}). It is believed that the slightly higher dislocation density in the 15% Al_2O_3 composite was associated with the non-uniform shape of the particulates in that material where the more angular reinforcements may lead to locally higher dislocation densities. The dislocation densities calculated for the materials studied here are about two orders of magnitude higher than those reported by Dutta *et al.* following a similar heat treatment [4]. However, dislocation density analysis of the micrographs presented by these workers indicate the dislocation densities are qualitatively similar to those observed here. Because the dislocation densities reported by these workers are similar to that expected in well-annealed materials, it is suggested that these workers may have erred in their calculations.

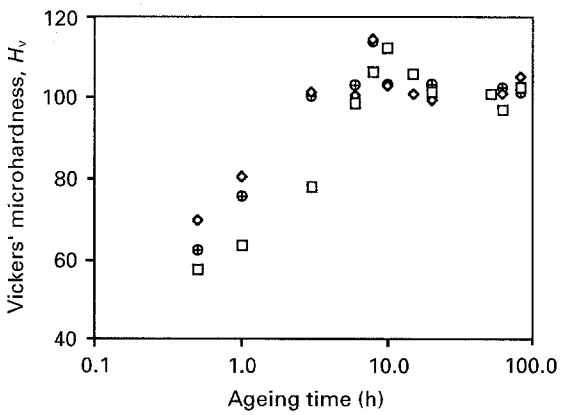

Figure 1 Microhardness as a function of ageing time at 175 °C for (□) the monolithic 6061 aluminium alloy, (◇) 15% Al_2O_3 and (⊕) Comral-85.

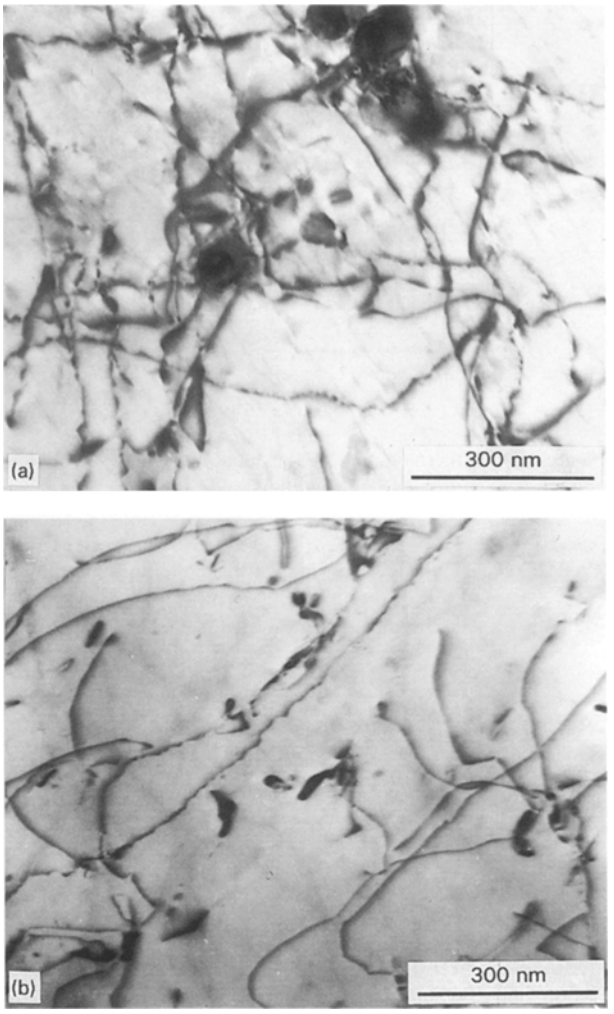

Figure 2 Bright-field transmission electron micrographs of (a) an area of the matrix adjacent to the particle in Comral-85 following solution treatment and quenching showing a high dislocation density, and (b) the matrix of the monolithic 6061 aluminium alloy following the same heat treatment.

In addition, a small number of undissolved particles (~0.5 μm diameter) were observed in all three materials studied in the solution-treated and quenched condition. EDS analysis indicated that they were rich in iron, silicon, magnesium and aluminium. This suggests that they are constituent intermetallics which are commonly observed in as-cast 6xxx series materials. However, no other particles were observed in these materials.

Thermograms were obtained from DSC scans of both the monolithic alloy and the composites on samples which were solution-treated and quenched. A detailed description of these thermograms has been published elsewhere [6]; however, a typical thermogram of the unreinforced 6061 Al alloy is shown in Fig. 3. The temperatures of all the peaks, whether exothermic or endothermic, for all five materials were identified and are summarized in Table II.

A typical DSC thermogram is given in Fig. 3, which is the thermogram for the monolithic alloy. Five exothermic peaks were observed: peak 1 at 102 °C, peak 2 at 172 °C, two overlapping peaks 4 and 5 at 272 and 322 °C, respectively, and peak 7 at 498 °C. In addition, three endothermic peaks were observed: peak 3 at 225 °C, peak 6 at 438 °C, and peak 8 at 530 °C. The thermograms obtained from the composites exhibited the same general form as this thermogram, except that the peaks occurred at slightly different temperatures and were of differing intensity.

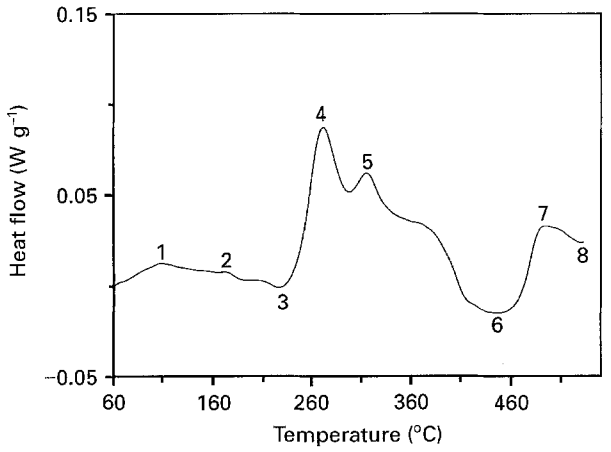

Figure 3 DSC thermograms of the monolithic 6061 aluminium alloy in the solution-treated condition.

Exothermic peak 1 appeared at the same temperature of 102 °C for all five materials. In each case this peak was very small, and no obvious change in intensity was noted between any of the materials. Fig. 4 shows transmission electron micrographs of samples of both the monolithic alloy and the two composites heated to 102 °C. In all three materials a number of very small precipitates are the characteristic feature of these micrographs. These precipitates were fully coherent with the matrix and they were visible only through strain contrast. The image characteristics of such precipitates were found to be similar to the coherent silicon clusters observed in Al–Si alloys by Ozawa and Kimura [15] and Dutta *et al.* both in 6xxx-based composites and the monolithic 6061 aluminium alloy [4, 16].

It was also noted that there were fewer silicon clusters in the composite matrices, and that these particles were slightly bigger than those observed in the monolithic alloy. Furthermore, the clusters in the composite appeared to form preferentially in regions of high dislocation density compared with a more even distribution of relatively finer silicon clusters in the monolithic alloy. Interestingly, Dutta *et al.* [4, 16] noted in their composites that silicon clusters formed during quenching from the prior solution-treatment temperature, but this did not occur in their monolithic alloy, and that during subsequent heat treatment, the presence of alumina resulted in a reduction in the intensity of the DSC peak associated with silicon cluster formation, such that it was no longer observed in the composite containing 15 vol % alumina. Furthermore, neither Papazian [1] nor Badini *et al.* [3] in similar studies observed a discrete peak associated with the formation of silicon clusters. Dutta *et al.* [4] suggested that the nucleation of silicon clusters is associated with the presence of quenched-in vacancy loops and

TABLE II Analysis of DSC scans of the monolithic 6061 aluminium alloy and composites in the solution-treated condition

Materials	Temperature of the peaks (°C)							
	Peak-1 Si[a]	Peak-2 GP-I[b]	Peak-3 DGP-I[c]	Peak-4 β″[d]	Peak-5 β′[e]	Peak-6 Dβ′[f]	Peak-7 β[g]	Peak-8 Dβ[h]
6061	102(+)[i]	172(+)	225(−)[j]	272(+)	322(+)	438(−)	498(+)	530(−)
10% Al_2O_3	102(+)	172(+)	225(−)	272(+)	308(+)	440(−)	492(+)	522(−)
15% Al_2O_3	102(+)	172(+)	225(−)	272(+)	305(+)	440(−)	485(+)	522(−)
20% Al_2O_3	102(+)	160(+)	225(−)	270(+)	298(+)	440(−)	485(+)	522(−)
Comral 85	102(+)	160(+)	225(−)	270(+)	305(+)	440(−)	488(+)	522(−)

[a] Formation of Si-clusters.
[b] Formation of GPI-zones.
[c] Dissolution of GP-I zones.
[d] Formation of β″ precipitates.
[e] Formation of β′ precipitates.
[f] Dissolution of β′ precipitates.
[g] Formation of β precipitates.
[h] Dissolution of β precipitates.
[i] Exothermic peak.
[j] Endothermic peak.

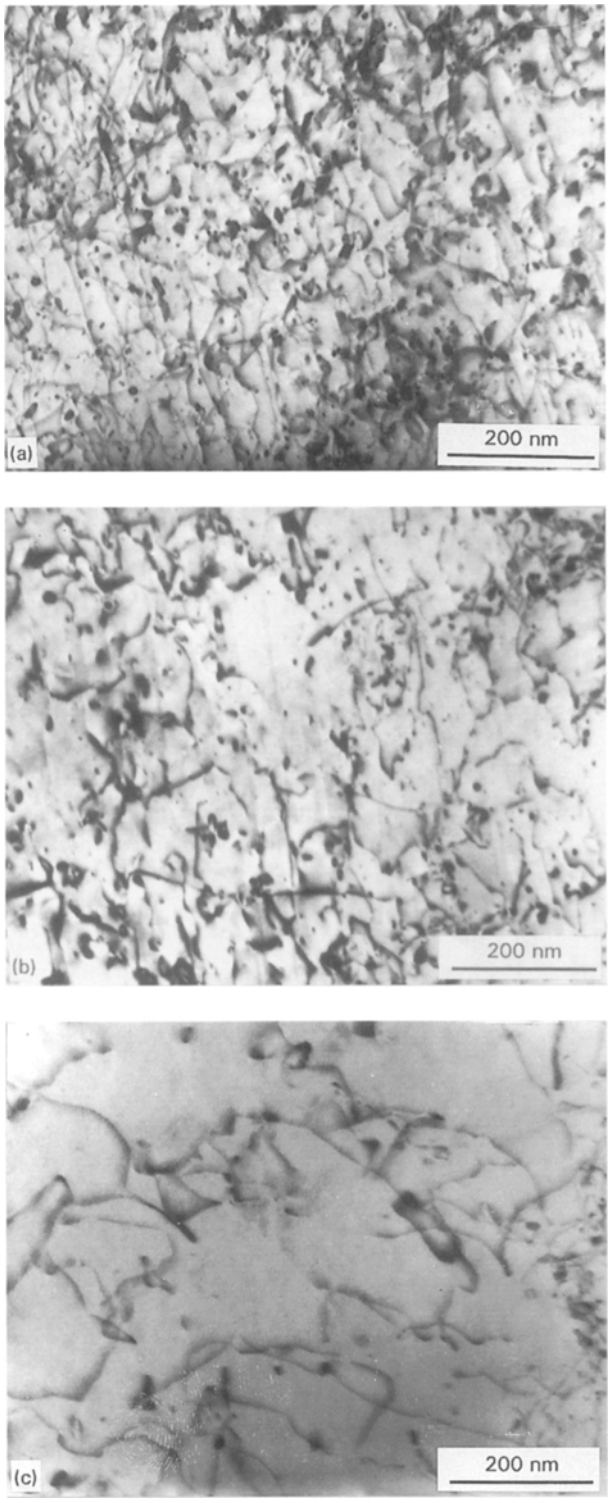

Figure 4 Bright-field transmission electron micrographs of (a) 6061 monolithic alloy, (b) 15% Al_2O_3 and (c) Comral-85 corresponding to peak 1 of the DSC thermogram.

CTE dislocations following the solution heat treatment. They suggested that larger numbers of CTE dislocations in the composite materials may have led to the formation of the silicon clusters during the quench in these materials. In the alloys studied here, silicon clusters were not observed in the as-quenched material. However, a smaller number of larger clusters was noted in the composites compared with the monolithic alloy.

It is clear that the conditions of formation of these silicon clusters is subject to considerable variation. It is known that the ageing behaviour of 6xxx alloys is highly sensitive to composition, especially the silicon and magnesium concentrations, and also the heat-treatment regimes used. Slight compositional differences between the materials studied here and those studied by other workers are apparent. Furthermore, other workers used a higher solution-treatment temperature than that used here which might be expected to produce both a higher vacancy concentration and a higher density of CTE-induced dislocations. These differences in material composition and heat treatment may account for any differences in behaviour which were observed.

Exothermic peak 2 appeared at 172 °C for both 10% and 15% Al_2O_3 6061 composites and the monolithic alloy. However, this peak appeared at a much lower temperature of 160 °C when the reinforcement content was increased to 20% for both the 20% Al_2O_3 and the Comral-85 composites. Furthermore, the peaks for both 10% and 15% Al_2O_3 6061 composites and the monolithic alloy were significantly smaller than those observed for the two composites which contained 20% Al_2O_3. Prior studies showed that this peak is associated with the formation of Guinier–Preston (GP-I) zones [3–6], and it can be inferred that a higher degree of reinforcement can both accelerate the kinetics of formation of GP-I zones and increase the proportion of this phase formed. However, it would seem that the shape and size of the reinforcements exerted little influence on the precipitation process at this stage as peak 2 occurred at the same temperature for both in 20% Al_2O_3 and Comral-85. These data are again in contrast to the work of Dutta *et al.* who demonstrated that additions of only 10% and 15% Al_2O_3 to 6061 decreased the peak temperature for GP-I formation although in their study the peak temperatures for formation of GP-I and GP-II zones were not clearly quantified because of obtaining an unresolved doublet for such formation.

Fig. 5 shows the microstructure of both the monolithic alloy and composites heated to the condition corresponding to peak 2 of their respective DSC thermograms. Two kinds of precipitates were noted. First, fine particles, which were believed to be the silicon clusters (labelled A, for example) associated with peak 1, and second a smaller number of particles (labelled B, for example), which exhibited strong strain contrast, with a line of no contrast normal to the diffraction vector operating on the foil plane. From the previous study on the DSC thermograms of these materials [3–6] and from prior studies of the precipitation sequence in Al–Mg–Si alloys [17–19], it can be inferred that these second particles are GP-I zones. Somewhat surprisingly, no clear difference in the density of the GP-I zones was noted in the three materials examined by TEM, although the relative proportion of GP-I zones in each material was generally low, making comparison difficult.

The endothermic peak 3, which from prior studies was thought to be associated with the dissolution of GP-I zones, appeared at the same temperature, 225 °C, for all materials. This is in contrast to the work of Badini *et al.* [3, 20] who showed that the addition of

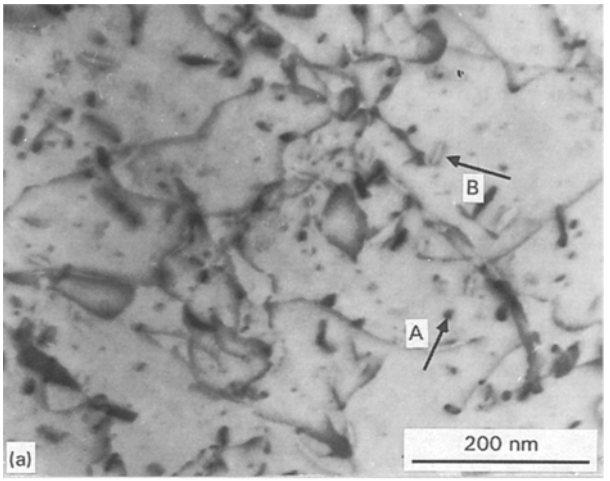

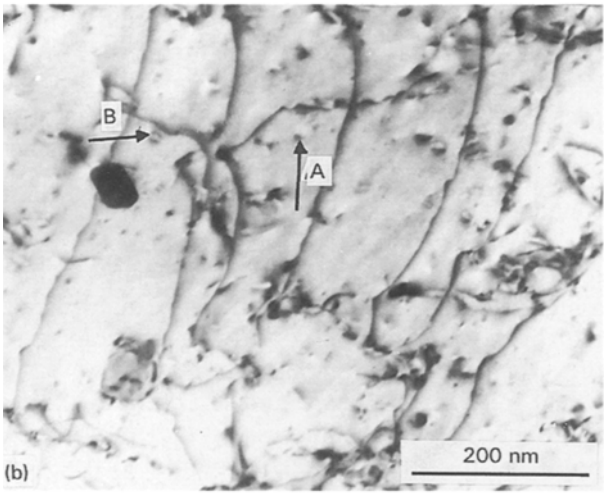

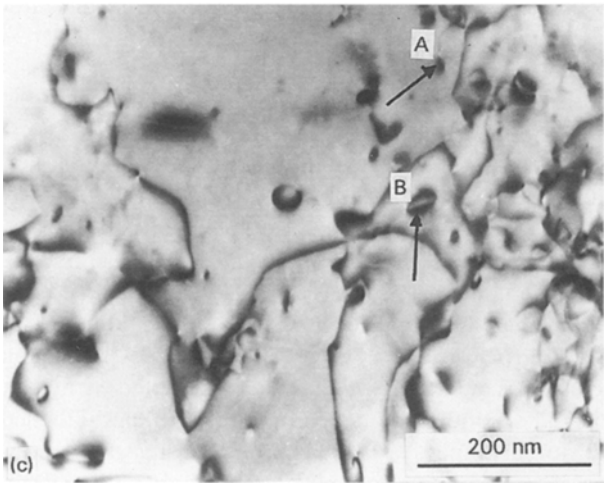

Figure 5 Bright-field transmission electron micrographs of (a) 6061 monolithic alloy, (b) 15% Al_2O_3 and (c) Comral-85 corresponding to peak 2 of the DSC thermogram.

about 17 vol % SiC whiskers and also 14 vol % SiC particulates to 6061 reduced the temperature of this peak from 228 °C to 200 °C. Again it is probable that differences in material composition and heat treatments given between this work and the work of Badini *et al.* may contribute to such differences. Fig. 6 shows a bright-field micrograph of the monolithic alloy heated to a temperature corresponding to the endothermic peak 3. Very few precipitates were observed, even under strong two-beam diffracting

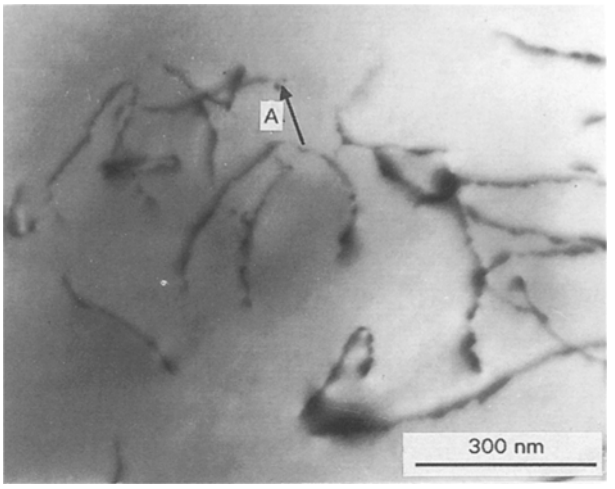

Figure 6 Bright-field transmission electron micrograph of 6061 monolithic alloy corresponding to peak 3 of the DSC thermogram.

conditions, suggesting that the dissolution of GP-I zones occur at this peak. However, a small number of GP-I precipitates (labelled A, for example) were still visible, indicating that the dissolution process was not complete. Similar microstructures were observed in both of the composite materials studied.

The third exothermic peak 4, associated with GP-II zone (or β″) formation, appeared at 270 °C for both 20% Al_2O_3/6061 and Comral-85 as compared with 272 °C for the monolithic alloy, 10% Al_2O_3 and 15% Al_2O_3. It was also noted that there was little difference in peak intensity for the five materials studied. However, peak 5, associated with formation of β′ appeared at 308, 305, 298 and 305 °C for 10%, 15%, 20% Al_2O_3 and Comral-85 composites, respectively, as compared to 322 °C for the monolithic alloy. It was also noted that as the volume fraction of reinforcement increased the intensity of this peak (4) decreased and the degree of overlap between peaks 4 and 5 increased. Thus, it is evident that the kinetics of formation of GP-II zones are little affected by the addition of reinforcements and the shape and size of the reinforcements appear to have no significant role in this type of precipitation. This is in contrast to Dutta *et al.* [4] who showed that increasing the volume fraction of reinforcement decreased the temperature of the GP-II zone peak, although they did not observe any clearly defined peak for GP-II zones as stated earlier. However, it is quite clear that the alumina particles accelerated the kinetics of β′ formation, which is consistent with the work of Dutta *et al.* Furthermore, the significantly lower temperature (298 °C) peak for the 20% Al_2O_3 composite, compared with the peak temperature (305 °C) for Comral-85, suggests that the smaller, angular-shaped reinforcements in this material may have exerted greater influence on the kinetics of precipitation of β′ phase. The relative decrease in the size of the β′ peak as the volume fraction of reinforcement increased, suggests that the slightly accelerated precipitation of β″ in the heavily reinforced composites may have inhibited the subsequent formation of β′.

Fig. 7 shows bright-field micrographs of samples heated to temperatures corresponding to peak 4 of the

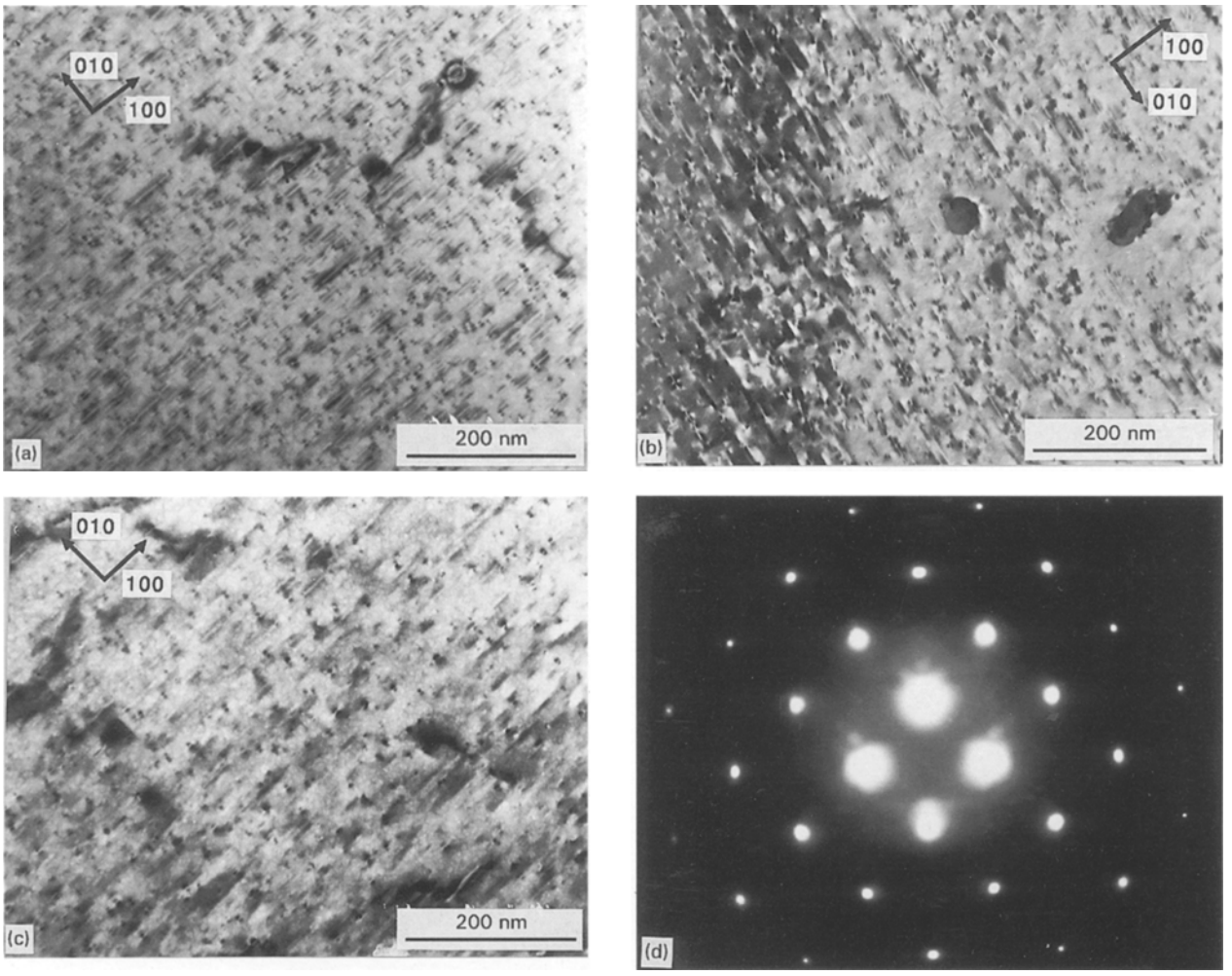

Figure 7 Bright-field transmission electron micrographs of (a) 6061 monolithic alloy, (b) 15% Al_2O_3 and (c) Comral-85 corresponding to peak 4 of the DSC thermogram; (d) $\langle 0\,0\,1 \rangle$ selected-area diffraction pattern from the matrix of the 6061 monolithic alloy.

DSC-thermograms of both the monolithic alloy and composites. The principal feature of these micrographs is needle-shaped precipitates about 20–25 nm long and 5–6 nm diameter aligned along the $\langle 1\,0\,0 \rangle$ matrix directions. These needles exhibited a line of no contrast under strong two-beam diffraction conditions normal to the diffraction vector. Selected-area diffraction patterns (SADP) exhibited streaking parallel to the $\{0\,0\,1\}$ planes (Fig. 7d), consistent with the observations of Dutta *et al.* [4], and other studies of 6xxx series precipitation sequences [21]. TEM examination of these alloys suggested that the β″ precipitates in Comral-85 were slightly larger than both the 15% Al_2O_3 composite and the monolithic alloy. This is consistent with the accelerated precipitation indicated by the DSC.

Fig. 8 shows transmission electron micrographs of the monolithic alloy and composite samples heated to peak 5; it is clear that the needles which appeared at peak 4 have coarsened to rods 150–200 nm long and about 10 nm diameter. Fig. 8d shows a $\langle 0\,0\,1 \rangle$ SAD pattern which again shows streaking parallel to $\{0\,0\,1\}$. Similar coarse rod-like precipitates have been identified as the metastable β′ by other workers [4, 7, 21]. Examination of the microstructures of these materials suggested that some of the β′ precipitates were slightly coarser in the composite compared with the monolithic alloy. This is consistent with the accelerated precipitation indicated by the DSC.

The strain fields associated with the formation of GP zones in 6061 aluminium alloys become progressively relieved during the precipitation process [21–24]. In composites, the high matrix dislocation density associated with differential thermal contraction increases with increasing reinforcement content. It was suggested by Dutta *et al.* [4] that the coherent and semi-coherent precipitates orient themselves such that the direction of maximum strain coincides with the Burgers vector of the host dislocation, which leads to a reduction in the associated strain energy. Because of the high dislocation density in the composite materials, a high fraction of the precipitates nucleate at dislocations, resulting in the acceleration of precipitation. Fig. 9 shows β′ precipitates in Comral-85 which have formed heterogeneously on dislocations, consistent with the suggestions of Dutta *et al.*

Peak 6, associated with the dissolution of β′ precipitates, showed similar behaviour to that for peak 3. That is, it appeared at 438 °C for the monolithic alloy as compared with 440 °C for all the composites. Fig. 10 shows bright-field micrographs of samples heated to peak 6 of their respective DSC thermograms. These micrographs show a duplex precipitate morphology consisting of relatively small β′ precipitates

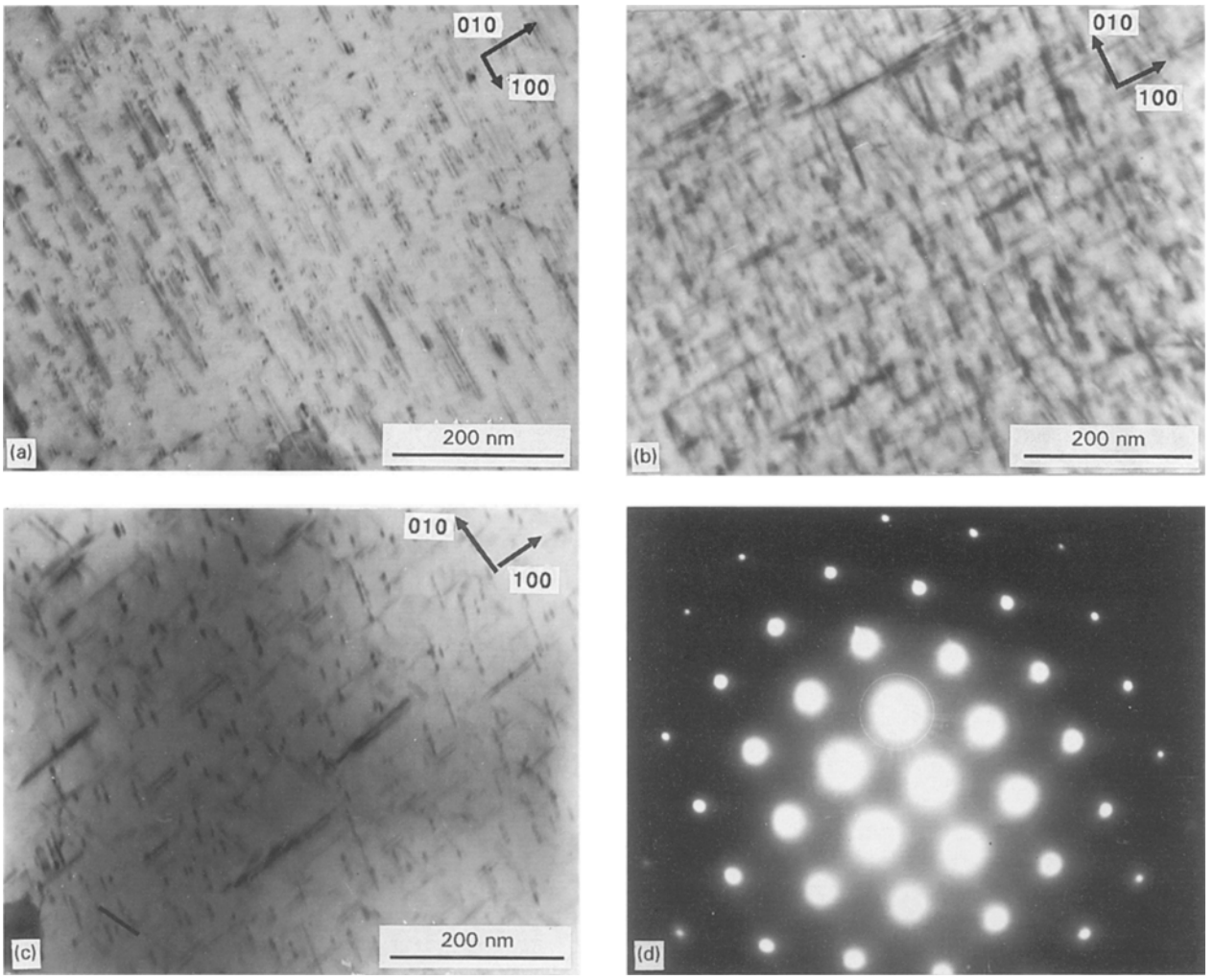

Figure 8 Bright-field transmission electron micrographs of (a) 6061 monolithic alloy, (b) 15% Al_2O_3 and (c) Comral-85 corresponding to peak 5 of the DSC thermogram (d) ⟨0 0 1⟩ selected-area diffraction pattern from the matrix of 6061 monolithic alloy.

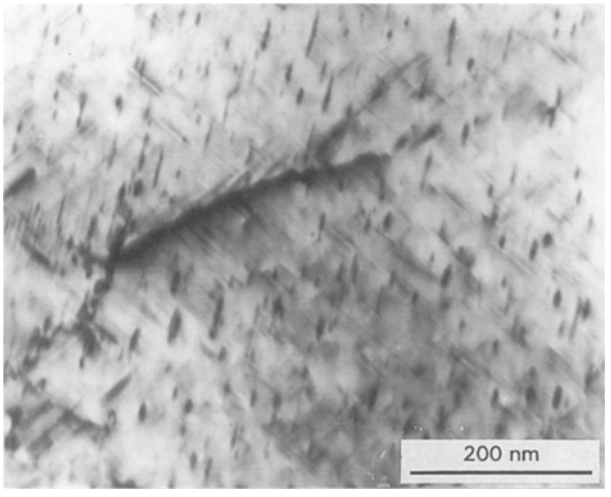

Figure 9 Bright-field transmission electron micrograph of a β′ precipitate associated with a dislocation in Comral-85 heat treated to conditions corresponding to peak 5 of the DSC thermogram.

and a limited number of large plate-like equilibrium β precipitates, suggesting that some of the rod-shaped β′ precipitates have started to grow into platelets of equilibrium β, whilst other β′ precipitates dissolve. In general, the precipitates in Comral-85 were larger than those in either the monolithic alloy or the 15% Al_2O_3 composite. This would suggest that the growth process is accelerated for Comral-85 compared with the other materials.

Peak 7, which is due to the formation β precipitates, appeared at 492, 485, 485 and 488 °C for 10% Al_2O_3, 15% Al_2O_3, 20% Al_2O_3 and Comral-85, respectively, as compared to 498 °C for their monolithic counterpart. Hence, the precipitation of β phase is also significantly accelerated by the reinforcement volume fraction, although the shape of the reinforcement does not seem to influence greatly this type of precipitation. Fig. 11 shows the bright-field micrographs of samples of the monolithic alloy and composites heated to peak 7 of their respective DSC thermograms. Plate-like precipitates 500–600 nm in length and 50–60 nm width, formed due to lateral coarsening of β′ precipitates, are the characteristic feature of these micrographs. Again, larger precipitates were observed in Comral-85. Jacobs [21] described such incoherent equilibrium precipitates as β phase having an f c c unit cell lattice with a parameter of $a = 0.639$ nm and similar to the CaF_2 structure. However, such precipitates were confirmed to be composed of magnesium and silicon by EDS analysis and this suggested the chemical formula of Mg_2Si [21, 23].

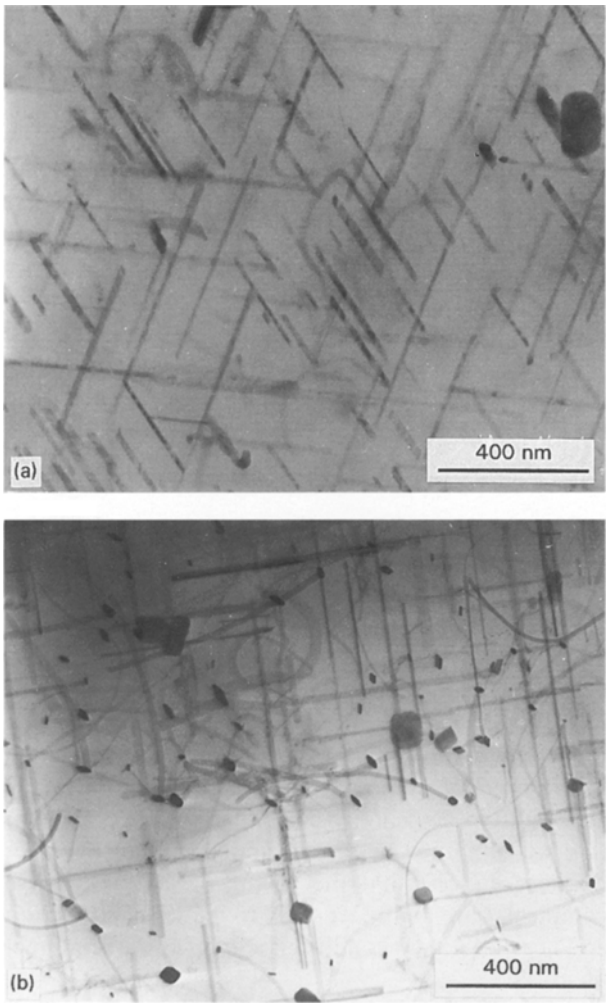

Figure 10 Bright-field transmission electron micrographs of (a) 6061 monolithic alloy, (b) 15% Al_2O_3 and (c) Comral-85 corresponding to peak 6 of the DSC thermogram.

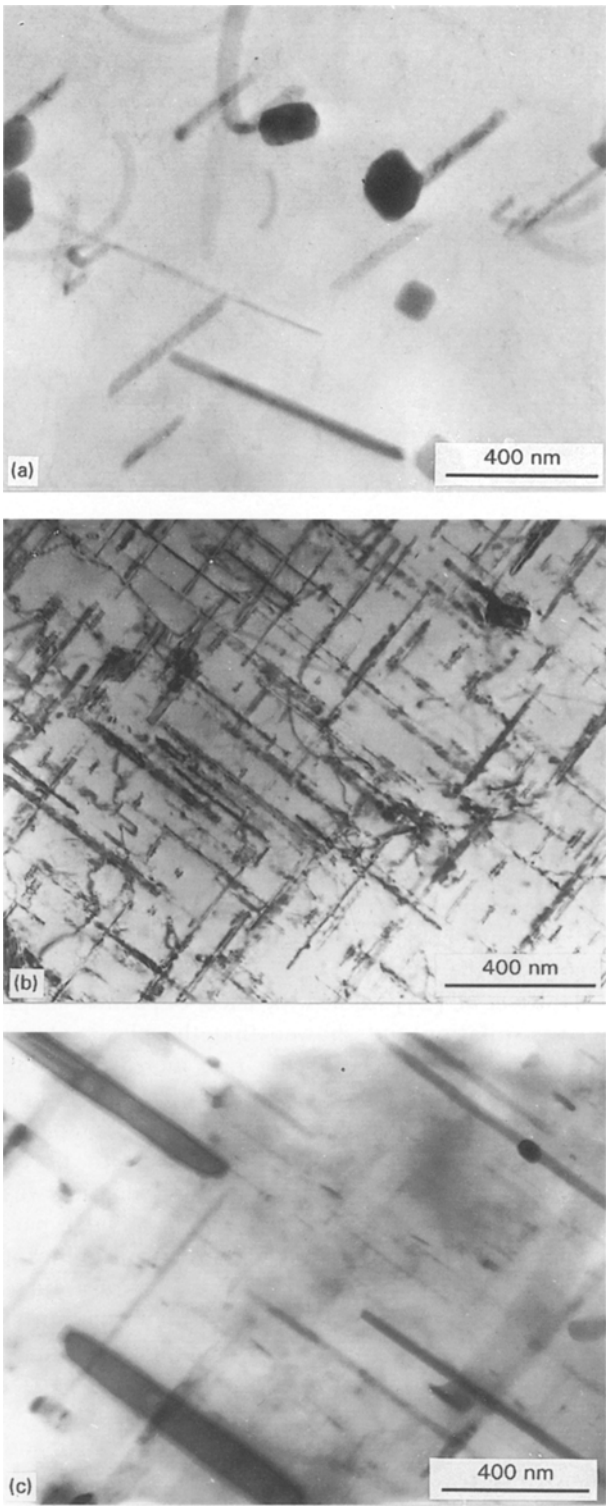

Figure 11 Bright-field transmission electron micrographs of (a) 6061 monolithic alloy, (b) 15% Al_2O_3 and (c) Comral-85 corresponding to peak 7 of the DSC thermogram.

Peak 8, associated with the dissolution of incoherent β precipitates appeared at 530 °C for the monolithic alloy, whereas the same peak appeared at a much lower temperature of 522 °C for all composites irrespective of the size, shape and volume fraction of the reinforcements. Hence it can be inferred that the dissolution of the β precipitates in the composites is accelerated due to addition of reinforcements in the matrix alloy. This is consistent with the DSC data of Dutta *et al.* [4], who suggested that dissolution occurred at a lower temperature for the composites than the monolithic alloy. Fig. 12 shows a bright-field micrograph of the monolithic alloy heated to the endothermic peak 8. No precipitates were observed at this stage, only some undissolved particles were present in the micrographs, which EDS analysis suggested were the constituent intermetallic phases described earlier. Similar microstructures were observed for both the composites studied.

It is clear from this study, that the trends observed here are broadly similar to those noted by other workers. That is, alumina reinforcements accelerate the ageing in 6xxx matrices, but that the precipitation sequence is the same for both the composites and the monolithic material. However, many slight differences in peak temperatures and the relative acceleration of various precipitation processes between this study and related studies on similar materials were noted. These inconsistencies regarding the peak temperatures for formation and dissolution of precipitates recorded by various workers may be attributable to the different processing history of the materials and also the different solution-treatment temperatures and quenching rates employed. Furthermore, slight differences in the chemical compositions of the matrices as well as differences in the size, shape and composition of the

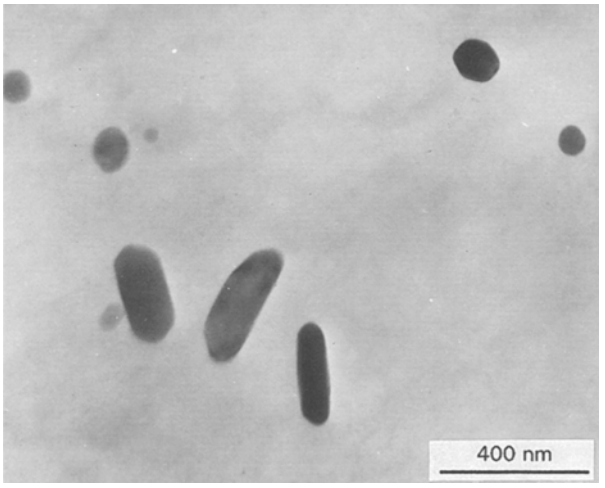

Figure 12 Bright-field transmission electron micrographs of 6061 monolithic alloy, corresponding to peak 8 of the DSC thermogram.

reinforcements, may have led to further differences in behaviour. In this respect, Papazian [1] showed that the precipitation behaviour of powder-metallurgy processed 6061 aluminium alloy and its composites is different compared to the wrought alloy.

The composites studied here contained a range of volume fractions of particulates from 10–20 vol%. In general, it was noted that any acceleration of the precipitation process was greater in the composites with the higher particulate content. This is in agreement with the work of Dutta *et al.* [4].

Dutta *et al.* [25] studied the effect of particle shape on precipitation and showed that the plastic strain and, consequently, the ageing rate increases as the reinforcing particulate aspect ratio increases and so spheres generate the lowest plastic strain compared to long cylinders, suggestive of whiskers or fibres. Although a slightly higher dislocation density was observed in the composite containing angular particulates rather than microspheres, no significant differences in the precipitation behaviour of these composites were observed except in the formation of β′ precipitates. Although any other differences may have been masked by differences in the average particulate size.

Recent work has been performed by Unsworth and Bandyopadhyay [8] and Hadianfard *et al.* [7] with composites containing spherical Al_2O_3 reinforcements. Unsworth's work, based on hardness measurement and TEM studies, showed the accelerated ageing phenomenon for the composite and a dual precipitate morphology consisting of GP zones and β′ precipitates at peak-aged (8 h at 175 °C) condition was observed. In another observation based on resistivity studies, Hadianfard *et al.* suggested that the accelerated precipitation in composites was due to the increased rates of nucleation and growth, and the nucleation is accelerated due to the reduction of incubation time for coherent precipitates at the initial stage. Also, it was reported in their study that the reinforcement addition can decrease the relative amounts of GP-I and GP-II zone formation with increased amounts of β′ and β precipitates, although no detailed microstructural observations were made in this study. This, however, contradicts the observations of Dutta *et al.* [4] and the present DSC study, where it was found that the proportions GP-I and GP–II zones increased with increasing reinforcement volume fraction, showing larger peak areas of such precipitates in the DSC thermograms. The intensities of the peaks for the formation of β′ and β precipitates decreased with increasing reinforcement volume fraction suggesting the decrease in the volume fraction of the respective phases with addition of reinforcements. This is consistent with the study made by Dutta *et al.* [4], but contradicts with the observation made by Hadianfard *et al.* [7].

4. Conclusion

A comprehensive calorimetric (DSC) investigation in conjunction with transmission electron microscopy (TEM) has been conducted on the precipitation and dissolution behaviour of Al_2O_3 particle-reinforced 6061 aluminium matrix composites. The presence of both angular and spherically shaped particles was observed significantly to accelerate age-hardening kinetics of the aluminium matrix alloy, although the precipitation sequence was not altered. Comparison of the data obtained here with similar studies by other workers, suggest that the ageing processes of these composites are highly sensitive to matrix composition and heat-treatment conditions as well as the reinforcement type.

References

1. J. M. PAPAZIAN, *Metall. Trans.* **19A** (1988) 2945.
2. P. APPENDINO, C. BADINI, F. MARINO and A. TOMASI, *Mater. Sci. Eng.* **A135** (1991) 275.
3. C. BADINI, F. MARINO and A. TOMASI, *J. Mater. Sci.* **26** (1991) 6279.
4. I. DUTTA, S. M. ALLEN and J. L. HAFLEY, *Metall. Trans.* **22A** (1991) 2553.
5. H. LEE, W. H. LU and S. L. I. CHAN, *Scripta Metall.* **25** (1991) 2165.
6. T. DAS, S. BANDYOPADHYAY and S. BLAIRS, *J. Mater. Sci.* **29** (1994) 5680.
7. M. J. HADIANFARD, Y-W MAI and J. C. HEALY, *ibid.* **28** (1993) 3665.
8. J. P. UNSWORTH and S. BANDYOPADHYAY, *ibid.* **29** (1994) 4645.
9. G. A. EDWARDS, G. L. DUNLOP and M. J. COUPER, in "3rd Australian Forum on MMC", Conference Proceedings University of New South Wales, Sydney, Australia, 7 December 1992, edited by S. Bandyopadhyay and A. G. Crosky (University of NSW, Sydney, 1992) p. 52.
10. T. G. NEIH and F. F. KARLAK, *Scripta Metall.* **18** (1984) 25.
11. J. L. PETTY-GALIS and R. D. GOOLSBY, *J. Mater. Sci.* **24** (1989) 1439.
12. M. D. SKIBO and D. M. SCHUSTER, US Pat. 475995, July 1988.
13. M. J. COUPER and K. XIA, in "Proceedings of the 12th Riso International Symposium on Materials Science: Metal matrix Composites – Processing, Microstructure and Properties", edited by N. Hansen, D. Juul Jenser, T. Leffers, H. Liholt, T. Loren-zen, A. S. Pedersen and B. Ralph (Riso National Laboratory, Denmark, 1991) p. 291.
14. T. DAS, S. BANDYOPADHYAY and S. BLAIRS, *J. Mater. Eng. Perform.* **1** (1992) 839.

15. E. OZAWA and H. KIMURA, *Mater. Sci. Eng.* **8** (1971) 327.
16. I. DUTTA and S. ALLEN, *J. Mater. Sci. Lett.* **10** (1991) 323.
17. V. A. PHILLIPS and J. D. LIVINGSTON, *Philos. Mag.* **7** (1962) 969.
18. H. CORDIER and W. GRUHL, *Z. Metalkde* **56** (1965) 669.
19. W. F. SMITH, *Metall. Trans.* **4** (1973) 2435.
20. C. BADINI, F. MARINO and A. TOMASI, *Scripta Metall.* **25** (1990) 57.
21. M. H. JACOBS, *Philos. Mag.* **26** (1972) 1.
22. H. J. RACK and R. W. KREZNER, *Metall. Trans.* **8A** (1977) 335.
23. G. THOMAS, *J. Inst. Metals* **90** (1961–62) 57.
24. D. W. PASHLEY, J. W. RHODES and A. SENDREK *ibid.* **94** (1966) 41
25. I. DUTTA and D. L. BOURELL, *Scripta Metall.* **22** (1988) 829.

Received 28 March 1995
and accepted 13 February 1996